CHAPTER 6. CHARACTERISATION OF THE MARTENSITIC TRANSFORMATION IN ARMOUR STEELS

6.1. Background

6.1.1 Theories of the martensitic transformation

A number of crystallographic and thermodynamic theories of the martensite transformation and the subsequent modifications to these theories have been briefly presented in Chapter 2. The Phenomenological crystallographic Theories of the Martensitic Transformations (PTMT) are concerned with the relationships that exist between the Bain strain, the invariant shape strain, the rotation and shear processes that comprise the so-called inhomogeneous or complementary strain. The original phenomenological approaches of Wechsler, Lieberman and Read (WLR) [102] and Bowles and Mackenzie (BM) [103] are equivalent. The first theory of WLR derived the shape strain as the result of the rotation R, the Bain distortion B and an inhomogeneous shear. The second theory of BM derived the total strain S which describes the homogeneous lattice strain occurring over a range of a few unit cells as the result of the shape strain and a complementary shear. Bowles and Mackenzie proposed that the complementary shear strain was part of a twinning shear in the martensite. This hypothesis implies that oppositely directed complementary shears could possibly produce twin orientations within a martensite plate, and it is well known that the plates produced in many martensitic transformations are twinned on a very fine scale. The Bowles and Mackenzie model predicts the crystallographic features such as the habit plane, the strain and the orientation relationships between the parent austenite and the product martensite.

The Phenomenological crystallographic Theories of the Martensitic Transformations have been successfully applied to many alloy systems, but as shown by Christian [45], in steels it can only be applied mainly to $\{2 \quad 5 \quad 9\}$ and $\{3 \quad 10 \quad 15\}$-type martensite plates; $\{2 \quad 2 \quad 5\}$ martensite plates and lath martensites have been proven difficult to fit to the theory. The concept of the displacement vector of the lattice deformation was then advanced by Gu et al [71]. They considered two ways to reduce the strain energy, i.e. the self-accommodation between different martensitic variants and plastic accommodation between the parent phase and martensite to explain the formation of $\{5 \quad 7 \quad 5\}$ martensite. Kelly [59] recently demonstrated that, when applied in a rigorous fashion, the Infinitesimal Deformation (ID) approach is exactly equivalent to the Phenomenological crystallographic Theory of the Martensitic Transformation (PTMT). The PTMT assumes the invariability of the habit plane. On the other side many researchers such as Christian [45], Kennon and Dunne [46], Tadaki and Shimizu [48], and Dunne and Kennon [49] have demonstrated that the flexibility of the habit plane is rather a characteristic of the martensite transformation than an exception.

In this study the PTMT model proposed by Bowles and Mackenzie was used for predicting the theoretical features of the martensite and their possible relation with the ballistic performance of the armour steels. The atom force microscopy is then used to find correspondences between the surface relief accompanying the martensitic transformation and the prediction by the Bowles and Mackenzie model of the PTMT. It can be accepted that an internally twinned martensite is mathematically equivalent to one that is internally slipped. That is, algebraically a predeformed austenite followed by the Bain deformation is equivalent to a martensite formed by the Bain mechanism followed by an inhomogeneous shear. When the martensite is not internally twinned, e.g. as in lath martensite, a single correspondence

relation and Bain deformation applies to an entire lath. In general, the reasons for a particular operative substructure (inhomogeneous shear) in a given material are rather obscure[69].
Zhang et al [98] have reported the results of many investigations made on the morphology transition from lenticular to butterfly to lath martensites. Variables reported to influence the martensite morphology include: transformation temperature, quench rate above M_s, chemical composition, dispersion of particles, thermodynamic driving force, austenite defect structure and stacking fault energy and the martensite and austenite strength. Davies and Magee [99] supposed that the morphology differences result from the different habit planes. The lattice invariant shear for the various martensite habit planes are as follows [99]:

$\{2 \quad 5 \quad 9\}$ - twinning in ferrite
$\{2 \quad 2 \quad 5\}$ - slip in austenite and twinning in ferrite
$\{1 \quad 1 \quad 1\}$ - slip in ferrite and austenite

These different habit planes usually correspond to lenticular, butterfly and lath martensites.

6.1.2. Tetragonality of martensite

The tetragonality of martensite in steels containing Carbon and Nitrogen is consistent with the correspondence implied by the Bain strain. Whereas in cubic ferrite the octahedral interstitial sites are occupied at random, in tetragonal martensite there must be a preferred occupancy of sites with only those octahedral sites along the martensite c-axes being filled, so producing the observed tetragonality. It was noticed in Chapter 2 that a significant redistribution of Carbon atoms and a disappearance of the tetragonality of a 5.1at.%C martensitic steel occurred at room temperature during aging times of less than 50 hours [66]. Carbon atoms segregated to lattice imperfections and also transferred from a/b-type octahedral interstices to c-type interstices, thereby decreasing the c_m parameter of the tetragonal martensite at room temperature.

Lyssak et al [67] have found that the tetragonality of the martensite in Manganese steels is abnormally small. Moreover, they have observed that there are several alloy systems in which the tetragonality of martensite containing Carbon, does not obey the well-known experimental equation:

$$c/a = 1 + 0.046\,p$$

where p is the mass percentage of Carbon in the steel. Kajiwara and Kikuchi [68] made a very extensive and systematic study of the martensite tetragonality in Fe-Ni-C alloys and found that the tetragonality is quite dependent on the mode of the lattice invariant deformation in the martensite.

Uehara et al. [69] have investigated the tetragonality of martensite in high Carbon- Iron alloys containing some Aluminium. From their study it appears that the tetragonality is enhanced by Aluminium and Nickel additions that prevent Carbon atoms from moving out of octahedral sites to tetrahedral sites during quenching (auto-tempering).

6.1.3. Techniques used in characterising the martensitic transformation

The features of the martensitic transformation may be determined by combining the determination of the phases present in the microstructure and their lattice parameters by the X-ray diffraction method, with the analysis of the morphologies, the spatial distribution and shapes of the phases determined by Transmission Electron Microscopy. Recently the introduction of Atomic Force Microscopy has brought in new possibilities of investigating the characteristics of the martensitic transformation by analysing the surface relief accompanying the transformation on a nanometric scale.

6.2. Characterisation methodology

(i) The inputs in the Bowles and Mackenzie model used in this study for the characterisation of the martensite are the lattice parameters of the martensite and of the retained austenite measured by X-ray diffraction at room temperature.
(ii) Complementary details on the martensite formation were determined by analysing the surface relief by Atomic Force Microscopy on a nanometric scale;
(iii) Scanning Electron Microscopy was used for analysis on a micrometric scale as complementary to the observation from the Atomic Force Microscopy; and
(iv) Transmission Electron Microscopy was used to determine the morphologies and the location of the phases that are present in the armour steels.

6.3. Characteristics of the martensite formation in the armour steels

6.3.1. Crystallographic characteristics

The volume fraction of the retained austenite and the lattice parameters of both the austenite and the martensite were determined by X-ray diffraction of the specimens austenitised at 900°C and quenched into water at room temperature. The martensite start temperatures were determined by dilatometric analysis. The crystallographic characteristics of the martensite formation were then calculated using the Bowles and Mackenzie model.

It was found from the XRD measurements of the lattice parameters that the martensite in these armour steels, is cubic with a_m approximately equal to c_m or, alternatively, it is possible that the tetragonality was so small that it could not be detected. Samples were double checked on two different XRD machines and were also stored at sub-zero temperatures between the quenching step and the XRD analysis to prevent significant Carbon movement. No tetragonality could be found. The measured lattice parameters and the calculated characteristics of the martensitic transformation in the nineteen armour steels are presented in Table (6.1).

The calculated magnitude of the complementary shear strain varies between 0.24 and 0.30 for these steels. The calculated misorientation from the Kurdjumov-Sachs orientation relationship is less than 1.2°. Nishiyama [36] estimated the limit of application of the calculated Kurdjumov-Sachs orientation relationship using the Bowles and Mackenzie model, to those cases where the calculated misorientation angle between the directions $\left[-1 \quad 0 \quad 1\right]_{\gamma}$ in the austenite and $\left[-1 \quad -1 \quad 1\right]_{m}$ in the martensite are smaller than 4°. According to this prediction the K-S orientation relationship may be applied to the martensite formation in these armour steels. Figure 6.1 illustrates the effect of the martensite start temperature on the scattering from the Kurdjumov-Sachs orientation relationship, on the complementary shear and on the magnitude of the displacement vector. It appears from this figure that the Kurdjumov-Sachs orientation relationship may be present in twinned as well as in lath martensitic armour steels.

Table (6.1). Lattice parameters and features of ferrous martensite in armour steels.

		Inputs								
Name of the armour steel	**Ms temperature [°C]**	a_γ **[nm]**	a_m **[nm]**	**Invariant line normal n**	**Complementary rotation Q**	**Total shape strain for the invariant line S**	**Invariant plane normal p1**	**Magnitude of the complementary shearm2**	**Shear angle [°]**	**Deviation from K-S [°]**
E	196	0.36448	0.2867291	0.4876 0.7243 0.4876	[1.0000 0 0 0 0.9876 -0.1073 0 0.1073 0.9876]	[1.0807 -0.0267 0.0973 0.0512 1.1188 0.0650 -0.1173 -0.1191 0.7667]	0.1984 0.6680 0.7172	0.28	8.19	0.94
F	255	0.36559	0.2863991	0.4769 0.7384 0.4769	[1.0000 0 0 0 0.9869 -0.1098 0 0.1098 0.9869]	[1.0751 -0.0266 0.0941 0.0496 1.1164 0.0659 -0.1109 -0.1194 0.7629]	0.1904 0.6511 0.7347	0.29	8.38	1.06
G	271	0.3683	0.2865805	0.4593 0.7604 0.4593	[1.0000 0 0 0 0.9858 -0.1138 0 0.1138 0.9858]	[1.0663 -0.0268 0.0889 0.0468 1.1122 0.0671 -0.1009 -0.1189 0.7570]	0.1780 0.6244 0.7605	0.30	8.68	1.27
H	210	0.36556	0.2862345	0.4756 0.7400 0.4756	[1.0000 0 0 0 0.9868 -0.1101 0 0.1101 0.9868]	[1.0744 -0.0266 0.0937 0.0494 1.1161 0.0660 -0.1101 -0.1194 0.7624]	0.1895 0.6491 0.7367	0.29	8.40	1.08
I	309	0.368300	0.286643	0.4598 0.7597 0.4598	[1.0000 0 0 0 0.9859 -0.1137 0 0.1137 0.9859]	[1.0666 -0.0268 0.0891 0.0469 1.1123 0.0671 -0.1012 -0.1190 0.7572]	0.1784 0.6253 0.7597	0.30	8.67	1.26
J	306	0.36652	0.2866597	0.4727 0.7438 0.4727	[1.0000 0 0 0 0.9866 -0.1108 0 0.1108 0.9866]	[1.0729 -0.0266 0.0929 0.0489 1.1154 0.0662 -0.1084 -0.1194 0.7614]	0.1874 0.6446 0.7412	0.29	8.45	1.11
K	318	0.36469	0.2864401	0.4835 0.7296 0.4835	[1.0000 0 0 0 0.9873 -0.1082 0 0.1082 0.9873]	[1.0786 -0.0266 0.0961 0.0506 1.1179 0.0654 -0.1148 -0.1193 0.7652]	0.1954 0.6616 0.7240	0.29	8.26	0.98
L	259	0.36475	0.286822	0.4865 0.7257 0.4865	[1.0000 0 0 0 0.9875 -0.1075 0 0.1075 0.9875]	[1.0802 -0.0267 0.0970 0.0510 1.1186 0.0651 -0.1166 -0.1191 0.7663]	0.1976 0.6663 0.7190	0.28	8.21	0.95
N	241	0.36468	0.2863646	0.4829 0.7304 0.4829	[1.0000 0 0 0 0.9873 -0.1084 0 0.1084 0.9873]	[1.0783 -0.0266 0.0959 0.0505 1.1178 0.0654 -0.1145 -0.1193 0.7650]	0.1949 0.6606 0.7250	0.29	8.27	0.99
O	218	0.36569	0.2863932	0.4761 0.7394 0.4761	[1.0000 0 0 0 0.9868 -0.1100 0 0.1100 0.9868]	[1.0747 -0.0266 0.0939 0.0495 1.1162 0.0660 -0.1104 -0.1194 0.7626]	0.1899 0.6499 0.7359	0.29	8.39	1.07
P	115	0.35837	0.285753	0.5211 0.6759 0.5211	[1.0000 0 0 0 0.9904 -0.0990 0 0.0990 0.9904]	[1.1002 -0.0293 0.1077 0.0551 1.1256 0.0618 -0.1392 -0.1146 0.7796]	0.2267 0.7252 0.6502	0.26	7.54	0.57
Q	178	0.35781	0.285086	0.5193 0.6788 0.5193	[1.0000 0 0 0 0.9902 -0.0995 0 0.0995 0.9902]	[1.0991 -0.0290 0.1071 0.0549 1.1252 0.0620 -0.1379 -0.1150 0.7788]	0.2249 0.7218 0.6546	0.26	7.58	0.59
R	170	0.36521	0.285806	0.4742 0.7418 0.4742	[1.0000 0 0 0 0.9867 -0.1104 0 0.1104 0.9867]	[1.0737 -0.0266 0.0933 0.0492 1.1158 0.0661 -0.1093 -0.1194 0.7620]	0.1885 0.6470 0.7388	0.29	8.43	1.09

S	182	0.35792	0.285704	0.5238 0.6718 0.5238	[1.0000 0 0 0 0.9906 -0.0984 0 0.0984 0.9906]	[1.1019 -0.0297 0.1085 0.0554 1.1261 0.0616 -0.1410 -0.1139 0.7807]	0.2292 0.7301 0.6438	0.26	7.49	0.55
T	184	0.36559	0.286066	0.4739 0.7422 0.4739	[1.0000 0 0 0 0.9867 -0.1105 0 0.1105 0.9867]	[1.0735 -0.0266 0.0932 0.0491 1.1157 0.0661 -0.1091 -0.1194 0.7619]	0.1882 0.6465 0.7394	0.29	8.4361	1.10
U	170	0.36486	0.286106	0.4794 0.7351 0.4794	[1.0000 0 0 0 0.9871 -0.1092 0 0.1092 0.9871]	[1.0764 -0.0266 0.0948 0.0500 1.1170 0.0657 -0.1123 -0.1194 0.7638]	0.1923 0.6550 0.7308	0.29	8.34	1.03
V	145	0.3578	0.2853	0.5212 0.6759 0.5212	[1.0000 0 0 0 0.9904 -0.0990 0 0.0990 0.9904]	[1.1002 -0.0293 0.1077 0.0551 1.1256 0.0618 -0.1392 -0.1146 0.7796]	0.2267 0.7252 0.6501	0.26	7.54	0.57
W	130	0.35819	0.285883	0.5235 0.6723 0.5235	[1.0000 0 0 0 0.9906 -0.0984 0 0.0984 0.9906]	[1.1017 -0.0297 0.1084 0.0553 1.1260 0.0616 -0.1408 -0.1140 0.7805]	0.2289 0.7295 0.6446	0.26	7.50	0.55

The higher martensite start temperatures led to larger angles between the directions $\left[-1 \quad 0 \quad 1\right]_{\gamma}$ and $\left[-1 \quad -1 \quad 1\right]_{m}$. For values of this angle larger than 4°, an intermediate orientation relationship between that of Kurdjumov-Sachs and Nishiyama-Wasserman may be found [36].

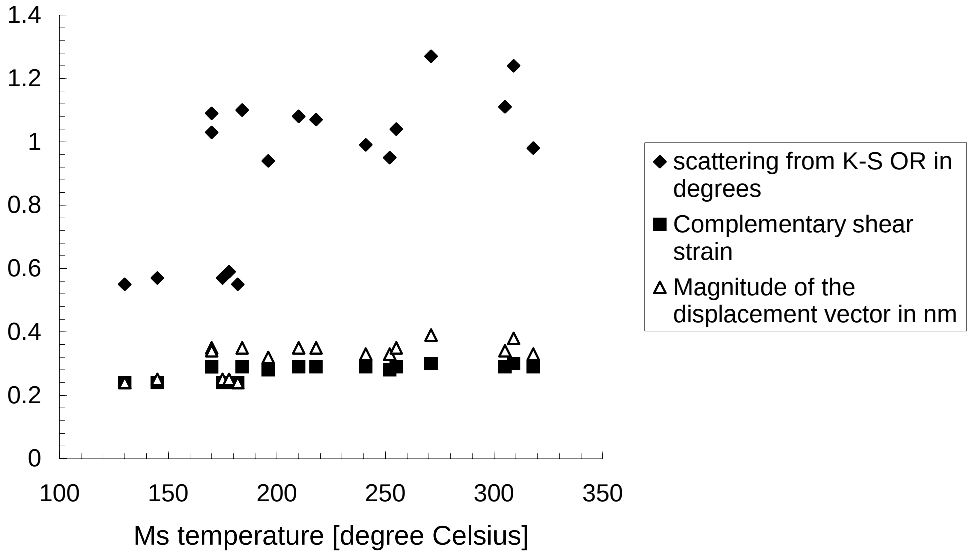

Figure 6.1: Dependence of the martensite formation characteristics on the measured martensite start temperature calculated by the Bowles and Mackenzie model.

The general trends of these characteristics present a plateau for the martensite start temperature within the range 200°C to 250°C. The values of these three characteristics are larger when the martensite start temperatures are higher than 250°C. The plateaux of intermediate constant values of the scattering from the Kurdjumov-Sachs orientation relationship, of the complementary shear strain and of the magnitude of the displacement vector may be explained by the equal probability of formation of the martensite by a slip or by a twinning mechanism in armour steels of which the martensite start temperatures range from 200°C to 250°C, contrary to the other two plateaux where one of the two mechanisms predominate at the expense of the other. The data collected by Morozov and co-workers [21] and presented in Table (2.5), show that many researchers have calculated the various parameters using different thermodynamic models and have predicted a change in the martensite formation mechanism at M_s temperatures between 232°C and 284°C for different Fe-C alloys. The plateaux of the crystallographic characteristics using the Bowles and Mackenzie model as presented in Figure 6.1, are in good agreement with these thermodynamic predictions. The variation in the morphology of the martensite in three armour steels is illustrated in Figure 6.2 for samples of steels H, G and I of which the martensite start temperatures were respectively 210°C, 271°C and 309°C, and that were austenitised at 900°C for 20 minutes in an argon atmosphere and then water-quenched to room temperature. The samples were then polished mechanically and etched for 7 seconds with a 2% Nital solution. In steel G whose martensite start temperature was 210°C, the martensitic structure consisted largely of plates coexisting with large laths.

The lath substructure became slimmer as the martensite start temperature became higher as illustrated in Figures 6.2 (a), (c) and (e) respectively for the three steels.

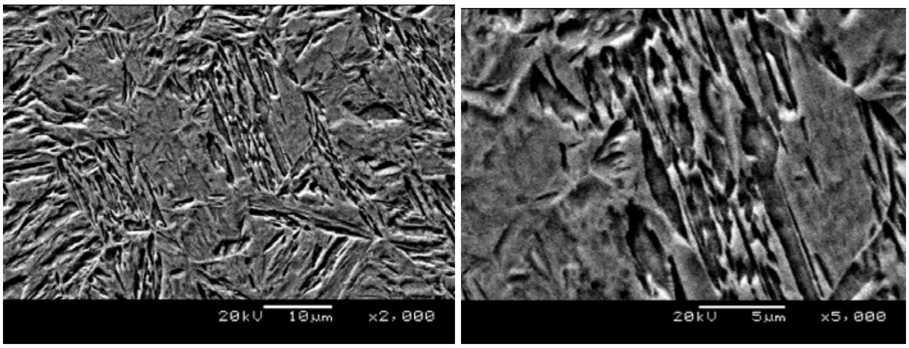

(a) (b)

Figure 6.2 (a) and (b): Backscatter scanning electron microscopy of steel G (M_S = 210°C). (a) x2000 and (b) x5000

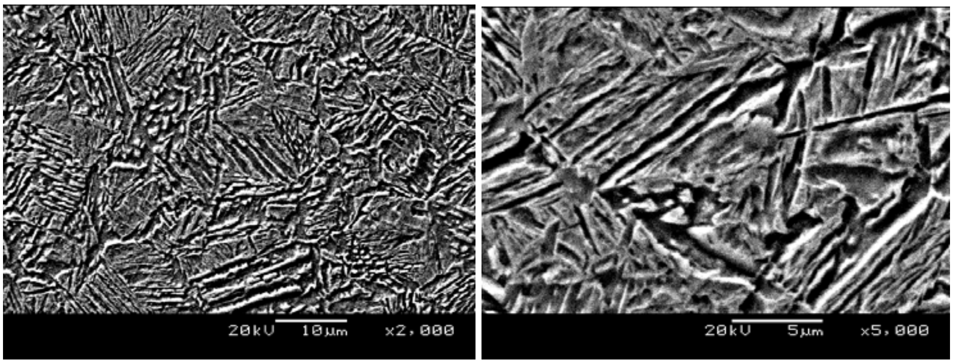

(c) (d)

Figure 6.2 (c) and (d): Backscatter scanning electron microscopy of steel G (M_S = 271°C). (c) x2000 and (d) x5000

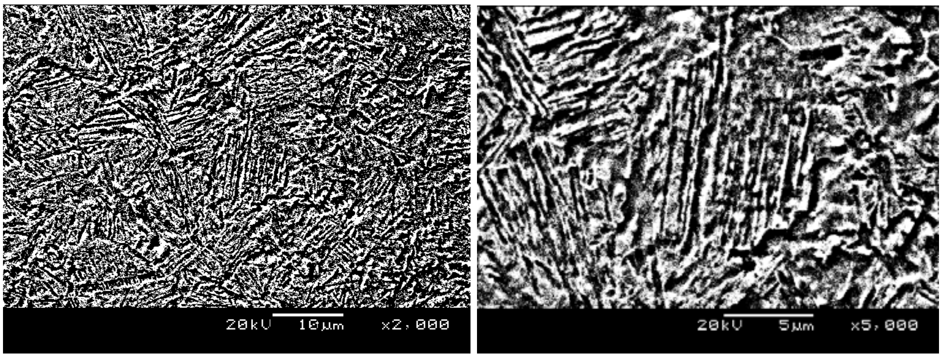

(e) (f)

Figure 6.2 (e) and (f): Backscatter scanning electron microscopy of steel I (M_S = 309°C). (e) x2000 and (f) x5000

The same observation was made by scanning electron microscopy of the samples when still unetched. Samples with thicknesses ranging from 1 to 2 mm were cut from the plates of steels E through to I, mechanically polished using a 1 micron diamond paste and cleaned 30 seconds in an ultrasonic cell containing pure ethanol.

These samples were then austenitised at 900°C for 10 minutes in a high vacuum atmosphere in the THETA Dilatometer and quenched to room temperature in a Helium-gas flow. The backscatter scanning electron microscopy micrographs of these samples are shown in Figure 6.3. The free-surface features of the martensite are coarser in steel E (shown in Figure 6.3(a)) which has the lowest martensite start temperature of 196°C and is finer in steel I (shown in Figure 6.3(e)) whose martensite start temperature is the highest at 309°C. The steels H, F and G whose martensite start temperatures were respectively 210°C, 255°C and 271°C, had intermediate sized free-surface martensite features as shown in Figures 6.3(b), 6.3(c) and 6.3(d) respectively. The small packets formed in steels whose martensite start temperatures are higher than 250°C, present less resistance against the combination of dynamic loading and localised high temperatures produced in zone 1 during ballistic impact.

It was noted in Chapter 4, that the free-surface martensite was not fully constrained during its formation as is the case inside the bulk of the steel, hence the differences in martensite plate widths between Figures 6.2 and Figure 6.3.

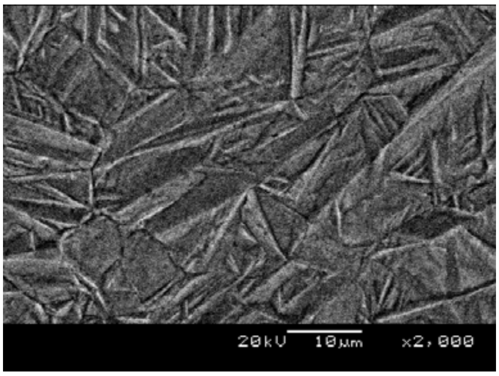

Figure 6.3(a): Backscatter scanning electron micrographs of steel E with M_s=196°C, finely polished before austenitising at 900°C for 10 minutes in high vacuum and quenched in a helium-gas flow. The sample was not polished or etched after quenching.

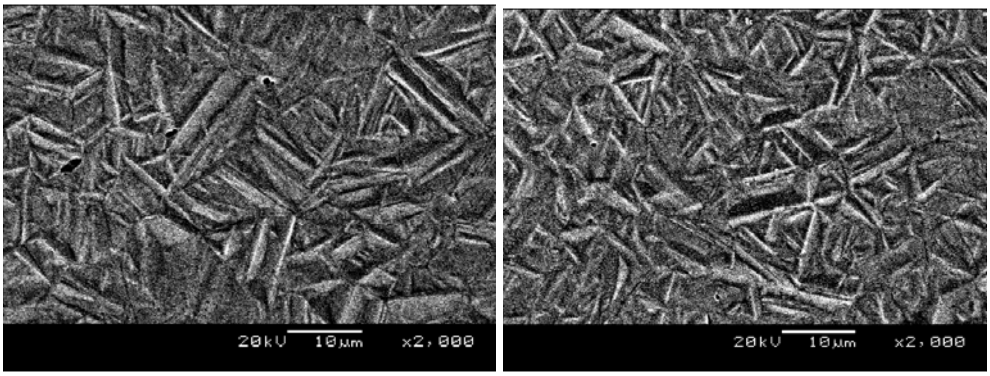

(b) **(c)**

Figure 6.3: (b) Backscatter scanning electron micrographs of steel H with M_s=210°C and **(c)** steel F with M_s=255°C, both finely polished before austenitising at 900°C for 10 minutes in high vacuum and quenched in a Helium-gas flow. The samples were not polished or etched after quenching.

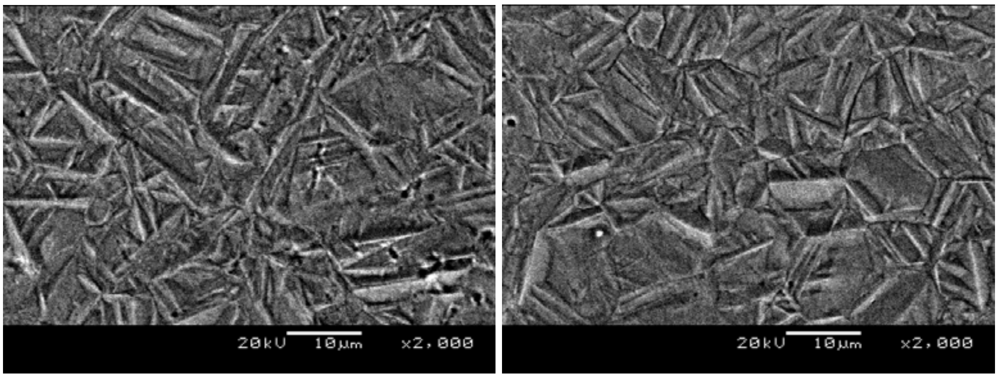

(d) **(e)**

Figure 6.3: (d): Backscatter scanning electron micrographs of steel G with M_s=271°C and **(e)** steel I with M_s=309°C, both finely polished before austenitising at 900°C for 10 in high vacuum and quenched in a Helium-gas flow. The sample was not polished or etched after quenching.

6.3.2. Quantitative analysis of the surface relief by means of Atom Force Microscopy

6.3.2.1: Plate martensite in steel E

Atomic Force Microscopy of steels E through to I was presented in Figure 4.4.36 of Chapter 4. The qualitative comparison of the surface relief apparently reveals different mechanisms of martensite formation in these steels. In Chapter 4, a qualitative classification of the surface relief of these armour steels was done according to their martensite start temperatures.

It was observed that in steel E which had a low martensite start temperature with M_s=196°C, internally twinned martensite formed by a shear mechanism accompanied by sub-twins. Two groups of twins were present and formed in two different directions A and B as shown in Figure 6.4. The twinning ratios of these two groups as well as their frequency were analysed using the Discrete Fourier Transform calculated by the Fast Fourier Transform algorithm of their spatial distributions and are compared in this paragraph.

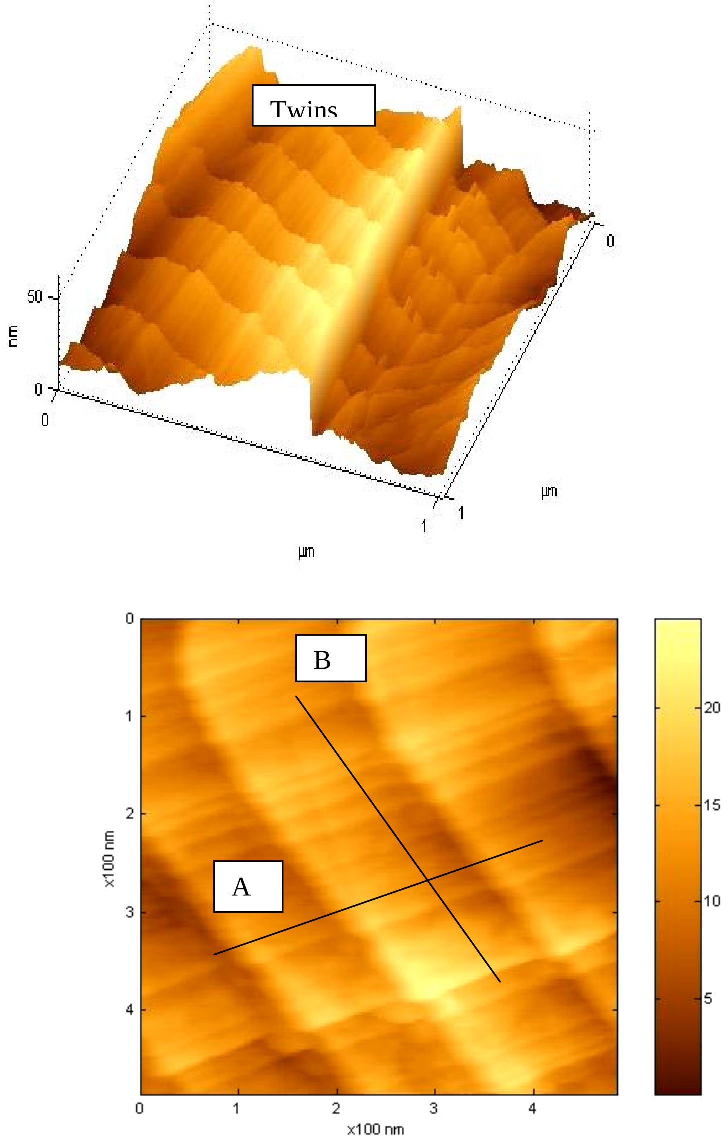

Figure 6.4: Atomic Force Microscopy of steel E with M_s=196°C, showing the twins (100 to 200 nm wide) and other finer parallel lines (sub-twins) approximately transverse to the twins (and approximately parallel to the habit plane)

Normal lines were considered relative to each direction A or B. The corresponding surface relief profiles along the two directions A and B with the corresponding Fast Fourier Transforms are illustrated in Figure 6.5 for the direction A and in Figure 6.6 for the direction B.

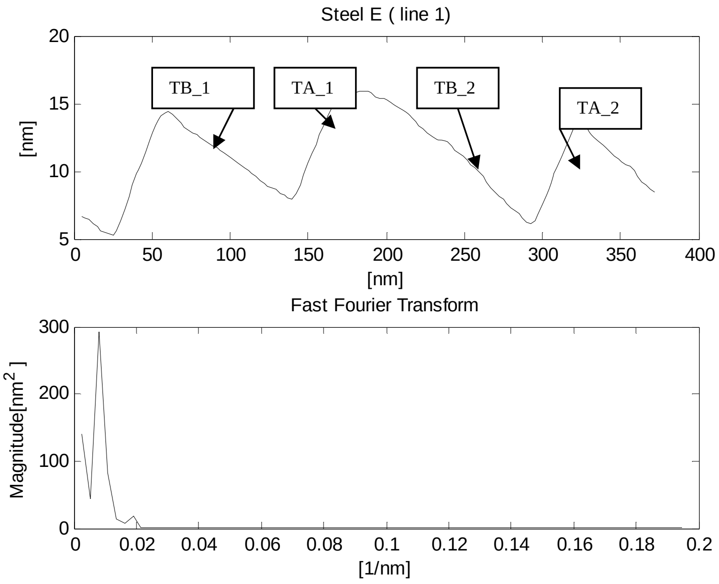

Figure 6.5(a): Surface relief profile of steel E along line 1 in the direction A and the corresponding Fast Fourier Transform

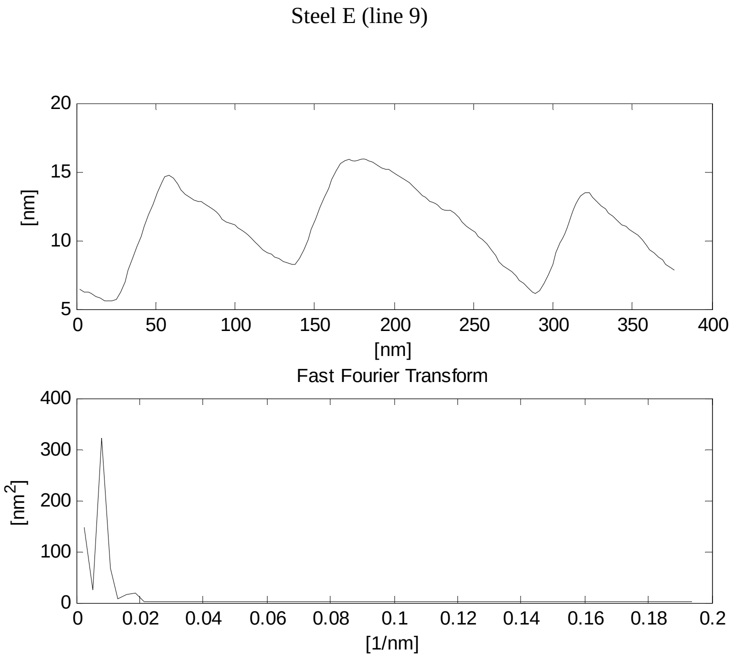

Figure 6.5(b): Surface relief profile of steel E along line 9 in the direction A and the corresponding Fast Fourier Transform.

The measured widths of the twins and the twinning ratios are presented in Table (6.2) and Appendix A6.2 where (dx) is the horizontal distance between a minimum and the following maximum or vice versa and (dy) is the height difference between the two points.

Table (6.2): Measured geometric characteristics of the twins along lines parallel to the direction A in steel E.

line 1	**TA_1**	**TB_2**	**TA_2**	**TB_3**	**TA_3**	
dx [nm]	35.71	79.61	33.48	24.55	95.98	
Height [nm]	9.05	-6.44	8.03	-8.75	7.35	
Relief angle [Degrees]	14.23	-4.62	13.50	-4.84	13.55	
Width [nm]	36.84	79.87	34.43	55.84	26.42	
Slope [nm/deg]	2.58	-17.25	2.54	-11.6	1.94	
Twinning ratio TB/(TB+TA)		0.69		0.68		
Line 9	**TA_1**	**TB_1**	**TA_2**	**TB_2**	**TA_3**	**TB_3**
dx [nm]	35.67	79.70	26.56	92.61	31.12	55.41
Height [nm]	9.17	-6.50	6.64	-9.06	7.37	-5.60
Relief angle [Degrees]	14.43	-4.66	14.04	-5.59	13.34	-5.78
Width [nm]	36.84	79.97	27.38	93.05	31.98	55.69
Slope [nm/deg]	2.55	-17.12	2.00	-16.63	2.39	-9.63
Twinning ratio TB/(TB+TA)	0.74		0.74		0.63	

The twinning ratio $\frac{TB\_i}{TB\_i + TA\_i}$ normal to the direction A in steel E spread from 0.6 to 0.81.

Twins TB_i are regular shapes whose relief angle is about 5.2±0.6°. Twins TA_i are rather regular shapes whose relief angle is about 13.5±2.0°.

The frequency spectrum contains a narrow bandwidth peak at about $0.008\,nm^{-1}$. This indicates that the plates are not exactly the same width but are rather continuously distributed around the mean width value which equalled $125\,nm$.

The surface relief profile along the direction B is illustrated in Figure 6.6.
The geometric measurement along the lines in the direction B are shown in Table 6.3. The twinning ratio $\frac{TB\_i}{TB\_i + TA\_i}$ along the normal to the direction B in steel E was spread within the range 0.55±0.03.

The surface relief was again N-shaped with twins TB_i whose relief angle was about 5.0±1.0° and twins TA_i whose relief angle was about 6.0±2.0°.

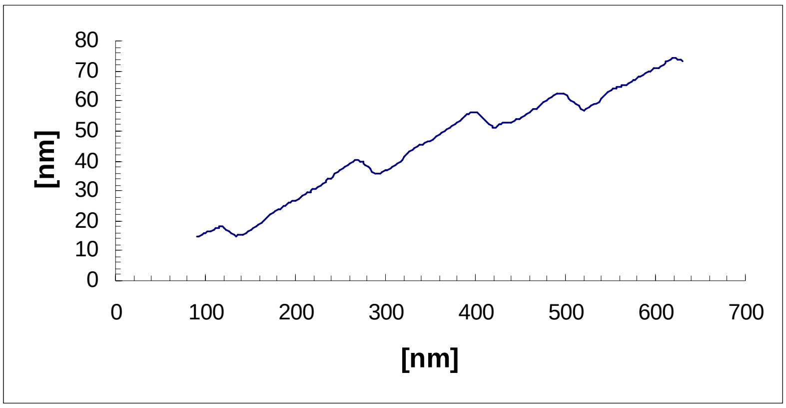

Figure 6.6(a): Typical surface relief profile along the direction B

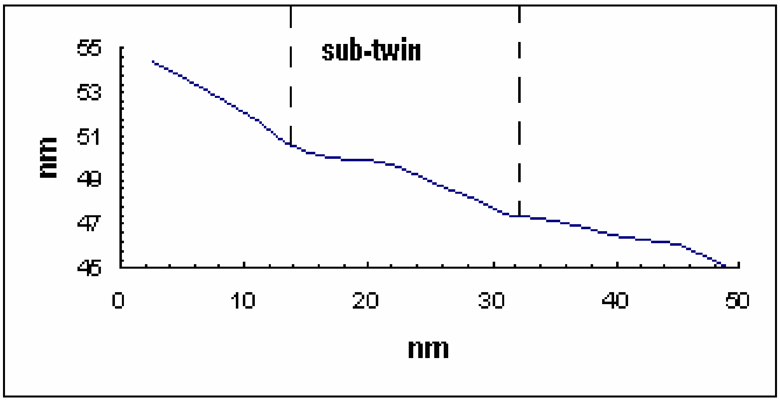

Figure 6.6(b): Typical surface relief profile of the sub-twins along the direction B

The total width of the sub-twin pairs normal to the direction B ranges from 10 to 20 *nm* which are smaller than 125 *nm* measured normal to the direction A.

Table (6.3): Measured geometric characteristics of the twins along lines in the direction B in steel E.

	TA_1	TB_2	TA_2	TB_3	TA_3	TB_4	TA_4
dx [nm]	42.03	48.32	33.62	31.52	27.32	52.53	37.82
height [nm]	3.29	-4.98	3.56	-2.73	1.13	6.59	-3.91
Relief angle [Degrees]	4.477	-5.89	6.05	-4.96	2.37	7.153	-5.91
Width [nm]	42.15	48.58	33.81	31.64	27.34	52.95	38.03
Slope [nm/deg]	9.414	-8.24	5.58	-6.37	11.49	7.40	-6.43
Twinning ratio TB/(TB+TA)		0.58		0.53		0.58	

The twinning ratio is also smaller normal to the direction B than normal to the direction A. Lin Xiaoping and co-workers [47, 96] have determined the crystallographic characteristics of the $\{2\quad 2\quad 5\}_\gamma$ and of the $\{2\quad 5\quad 9\}_\gamma$ martensite in a Fe-23%Ni-0.55%C and a Fe-8%Cr-1%C alloy respectively using Atomic Force Microscopy.

They have observed that the relief angles of the $\{2\quad 5\quad 9\}_\gamma$ and the $\{2\quad 2\quad 5\}_\gamma$ martensite range respectively from 4 to 5.8° and from 1 to 9°. The relief angles measured for steel E which ranged from 4 to 6°, was in good agreement with those measured by Lin Xiaoping and co-workers for the $\{2\quad 2\quad 5\}_\gamma$ martensite. However the widths of the plates measured for steel E ranging from 90 to 125 nm, were at least two times smaller than those measured by Lin Xiaoping and co-workers [95]. It seems from this comparison that the relief angle of the $\{2\quad 2\quad 5\}_\gamma$ martensite may be less sensitive to the chemical composition than the width of the plates.

The austenitisation temperature seems to have an effect on the widths of the plates but not on the relief angles. Indeed, the data from Table 1 of the work done by Lin Xiaoping and co-workers [95] shows that the heights and the widths of the plates increase when the austenitisation temperature increases from 1173K to 1473K.

A number of areas of the steel E consist of zigzag-shaped, while the rest consisted of twin martensite. The adjacent plates of zigzag-shaped martensite share the same conjugate habit plane. According to the Nishiyama-Wasserman-I (NW-I) and Nishiyama-Wasserman-II (NW-II) orientation relationships, the adjacent plates that share the same conjugate habit plane may grow in two symmetrical directions, so a tent-shaped surface relief is formed by their mutually back-to-back accommodation growth [93].

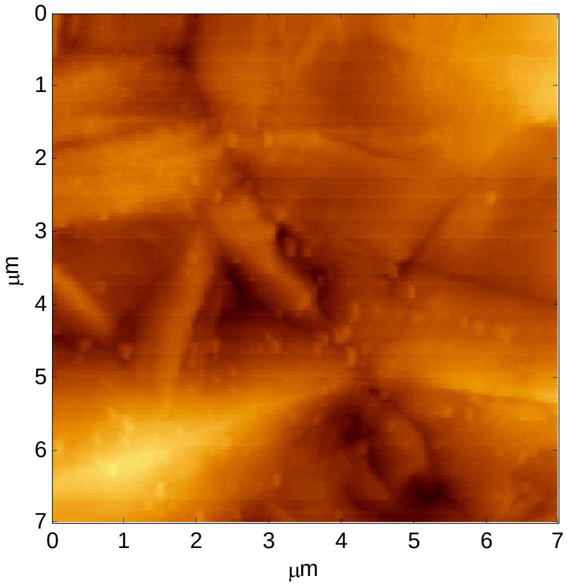

Figure 6.7: Zigzag-shaped martensite appears to have been formed in some parts of steel E

6.3.2.2: Lath martensite in the steel I

The martensite start temperature of steel I is 309°C. Figure 4.4.35(e) of Chapter 4 showed the thin foil TEM bright field image of this steel. Lath morphology of the martensite in this steel was found after austenitisation at 900°C for 20 minutes and water quenching. Figure 6.8 illustrates the surface relief accompanying the martensite formation in this steel. Contrary to steel E's surface relief, is that of steel I irregular and N-shaped, which is not in agreement with the prediction of the invariant plane strain [95, 96].

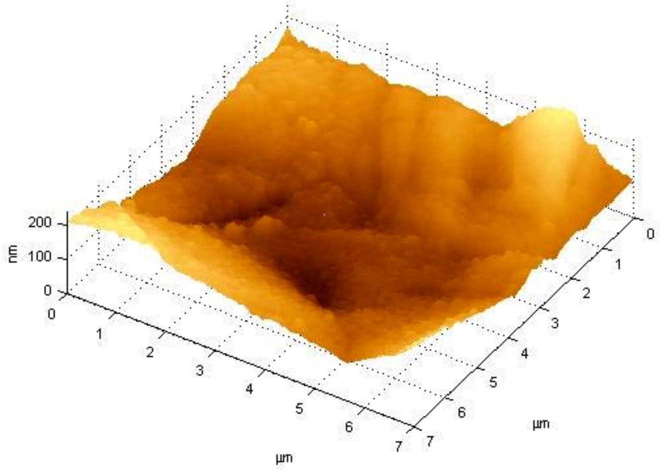

Figure 6.8 (a): Surface relief accompanying the formation of slipped martensite in steel I showing the irregular N-shape.

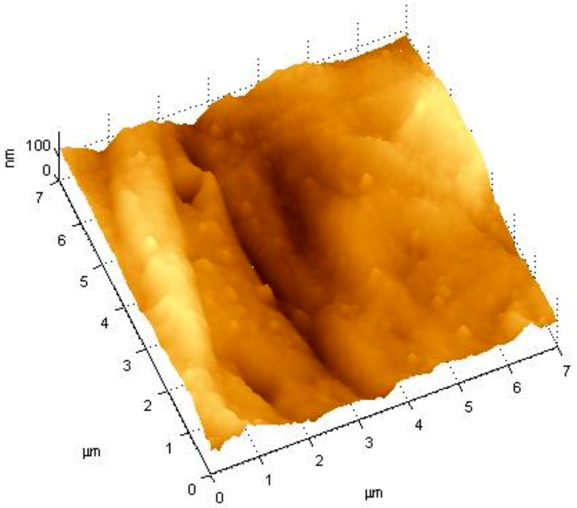

Figure 6.8 (b): Surface relief accompanying the formation of slipped martensite in steel I (Ms =309°C) showing the irregular N-shape.

A typical surface relief profile accompanying the formation of the martensite in steel I is illustrated in Figure 6.9. Relief deterioration is possible in the case of this relatively high Ms temperature through thermal smoothing and oxidation.

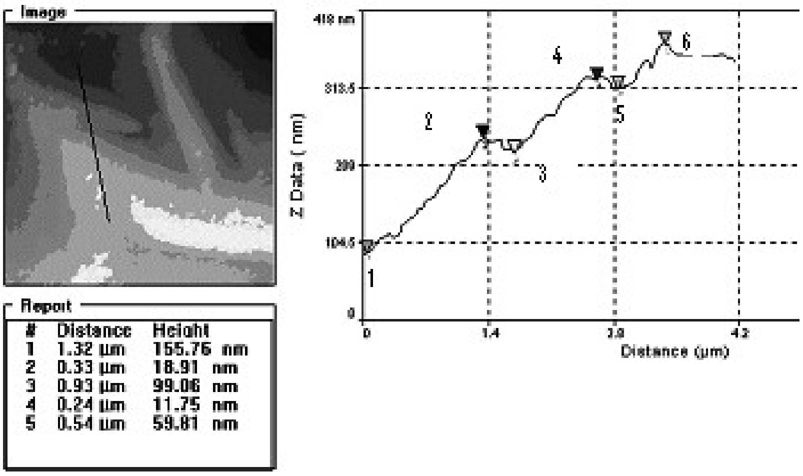

Report

#	Distance	Height
1	1.32 µm	155.76 nm
2	0.33 µm	18.91 nm
3	0.93 µm	99.06 nm
4	0.24 µm	11.75 nm
5	0.54 µm	59.81 nm

Figure 6.9: Typical surface relief profile after martensite formation in steel I and the corresponding geometric characteristics. The number in the first column indicates the segment number, i.e. 1 correspond to segment 1-2, 2 corresponds to segment 2 –3.

The laths are larger than 1.1 µm. This is about 2 times the width of the martensite plates formed in steel E. The size of the laths or of the plates may have an effect on the effective "grain size" in resisting fracture or perforation due to ballistic impact.

The transition of the martensite morphology in the armour steels as determined by Atomic Force Microscopy was illustrated in Figure 4.4.36 of Chapter 4. AFM images reveal three different morphologies of the martensite formed in these armour steels depending on the specific martensite start temperatures. Based on the work of Davies and Magee [99], the AFM results presented in Figure 4.4.36 and the crystallographic parameters using the Bowles and Mackenzie model as presented in Table (6.1) and Figure 6.1, the lattice invariant shear for the various martensite habit planes for the armour steels E through to I would be as follows:

Table (6.4): Habit planes of the armour steels E through to I as defined using the AFM results, the work of Davies and Magee and the crystallographic parameters from the BM model

	M_S [°C]	Illustrated in	Habit plane	Invariant lattice shear angle [°]	Total strain
Steel E	196	Figure 4.25(a)	{2 2 5}- twinning in ferrite	8.19	0.28
Steel H	210	Figures 4.25(b); 6.2(a)		8.40	0.29
Steel F	255	Figure 4.25(c)	{2 2 5}and {5 7 5} slip in austenite and twinning in ferrite	8.38	0.29
Steel G	271	Figures 4.25(d); 6.2(c)		8.48	0.30
Steel I	309	Figures 4.25(e); 6.2(e)	{5 7 5} or{1 1 1}- slip in austenite and ferrite	8.47	0.30

6.4. Orientation relationship between martensite and retained austenite

The orientation relationship between martensite and retained austenite in the armour steels W (M_s =130°C), U (Ms =170°C), and H (M_s =210°C), were determined by the electron diffraction technique. It is concluded in Figure 6.10 that, in the Steel W, the orientation between the martensite and the retained austenite obeys the Nishiyama-Wasserman orientation relationship with:

$$\begin{aligned}(1 \quad 0 \quad 0)\alpha \,//\, (1 \quad 1 \quad 0)\gamma \\ \langle 0 \quad 1 \quad 1\rangle\alpha \,//\, \langle 1 \quad \bar{1} \quad 1\rangle\gamma\end{aligned}$$

Figure 6.10(a): TEM thin foil bright field of the steel W (Ms = 130°C). Label mark: 500 nm

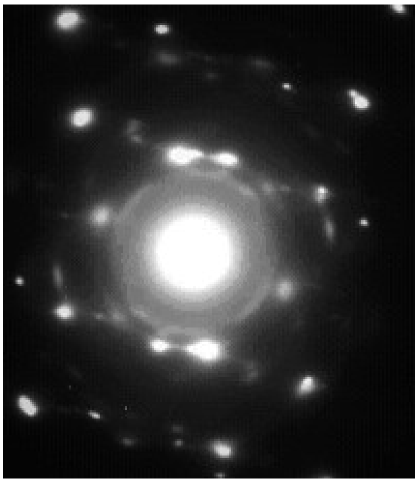

Figure 6.10(b)

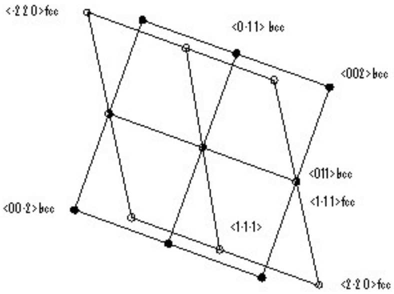

Figure 6.10c

Figure 6.10(b): Selected Area Diffraction Pattern from Figure 6.10(a). **Figure 6.10(c)**: Corresponding indexing

The dark field images corresponding to the spots $\langle 0\ \ \bar{1}\ \ 1\rangle bcc$ and $\langle \bar{2}\ \ 2\ \ 0\rangle fcc$ are shown in Figure 6.10(d) and 6.10(e) respectively.

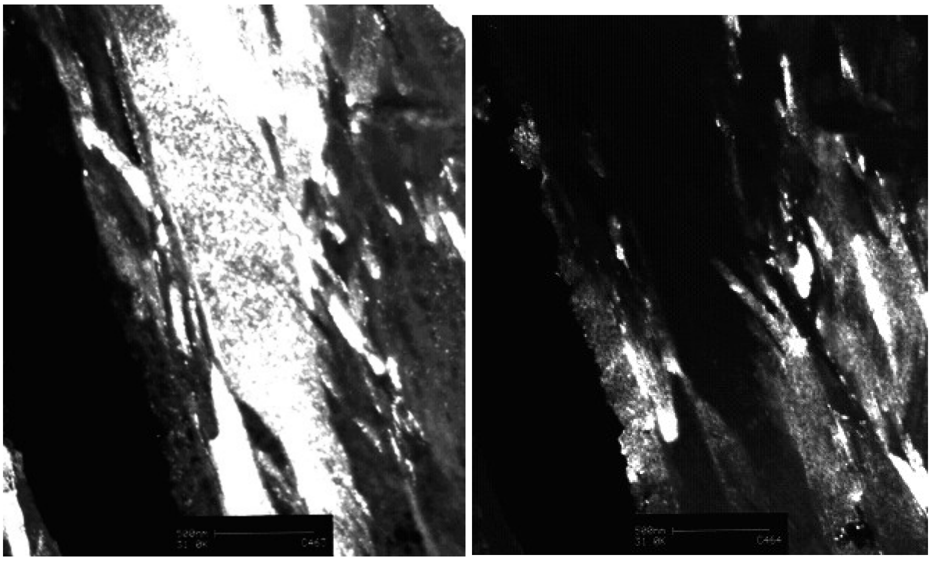

Figure 6.10(d) **Figure 6.10(e)**

Figure 6.10(d): TEM thin foil dark field image corresponding to the spot $\langle 0\ \ \bar{1}\ \ 1\rangle bcc$ showing the martensitic matrix. **Figure 6.10(e):** TEM thin foil dark image corresponding to the spot $\langle \bar{2}\ \ 2\ \ 0\rangle fcc$ showing nodular retained austenite. Label mark: 500 nm

The same orientation relationship was observed in the Steel U, with M_s = 170°C. The typical TEM thin foil bright image of this steel is shown in Figure 6.11(a).

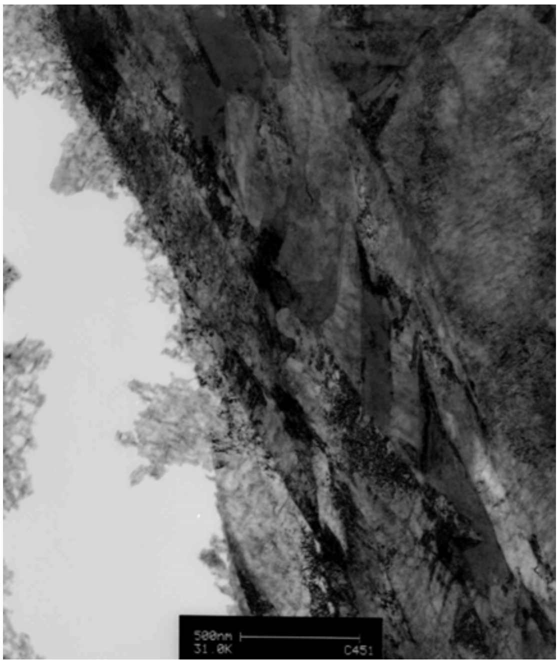

Figure 6.11(a): TEM selected area bright field of the steel U. Label mark: 500 nm

The Selected Area Diffraction Pattern and the indexing map of this steel are presented in Figure 6.11(b) and 6.11(c).

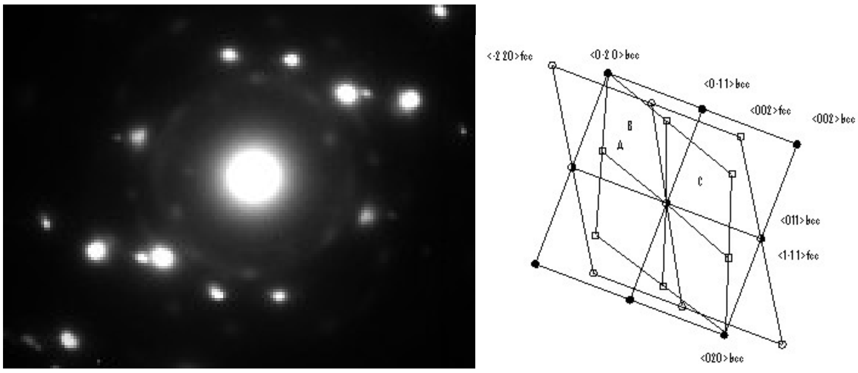

Figure 6.11(b) **Figure 6.11(c)**

Figure 6.11(b): Typical SADP of the Steel V, M_s = 145°C. **Figure 6.11(c):** corresponding indexing map.

It is concluded from this mapping that the Nishiyama-Wasserman orientation between the parent austenite and the martensite is obeyed in this steel.

$$(1 \quad 0 \quad 0)\alpha // (1 \quad 1 \quad 0)\gamma$$
$$\langle 0 \quad 1 \quad 1 \rangle \alpha // \langle 1 \quad \bar{1} \quad 1 \rangle \gamma$$

The spacing of the planes that produced the extra spots A, B and C are close to the lattice parameters of cementite, however the corresponding angles differ by about 2°. They may be formed by the reflexions from a structure that is very close to the orthorhombic cementite, possibly an iron carbide formed by autotempering during the quenching.

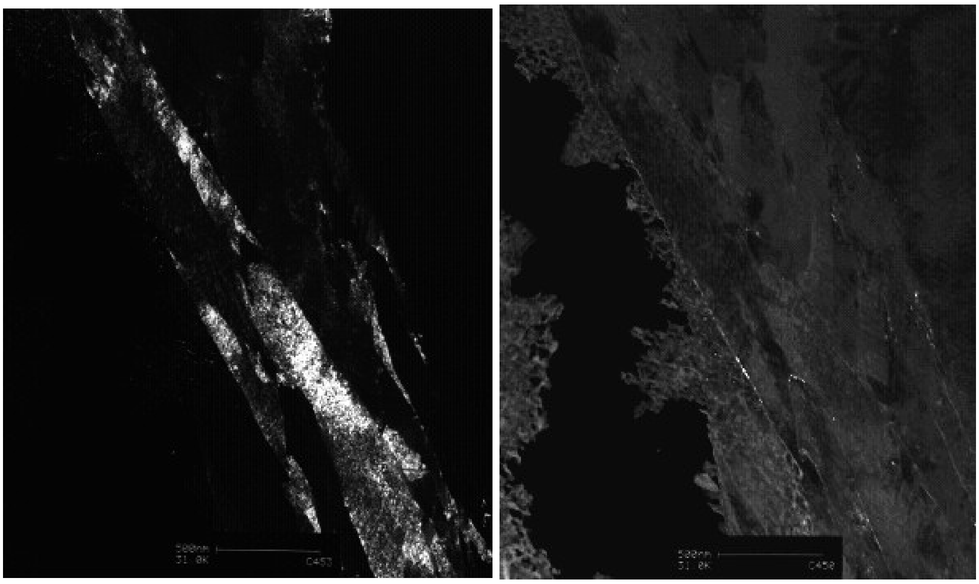

Figure 6.11(d) **Figure 6.11(e)**

Figure 6.11 (d) and **(e):** TEM dark field images corresponding to the spots $\langle 0\ \bar{1}\ 1\rangle bcc$ showing the martensitic matrix and $\langle \bar{2}\ 2\ 0\rangle fcc$ revealing the retained austenite along the martensite twinned plates. Label mark: 500 nm

Formatted

In steel H, M_s = 210°C, the SADP presents the orientation relationship

$$(1\ 0\ 0)\alpha // (1\ 1\ 2)\gamma$$
$$\langle 0\ 1\ \bar{1}\rangle \alpha // \langle 1\ \bar{1}\ 1\rangle \gamma$$

which deviates from the Nishiyama-Wasserman by 7°.

In this steel also the spacing of the planes that produced the extra spots A,B,C,D and E are close to those of cementite and suggest the possibility of autotempering and the formation of fine carbide particles of a carbide such as $Fe_{2.4}C$ or ε-carbide.

Figure 6.12(a) presents a typical TEM thin foil bright field image of the steel H. The SADP corresponding to the region near the boundary indicated with an arrow, is shown in Figure 6.12(b) and the indexing map in Figure 6.12(c).

Figure 6.12(a): TEM selected area bright field of the steel H (M_s = 210°C)

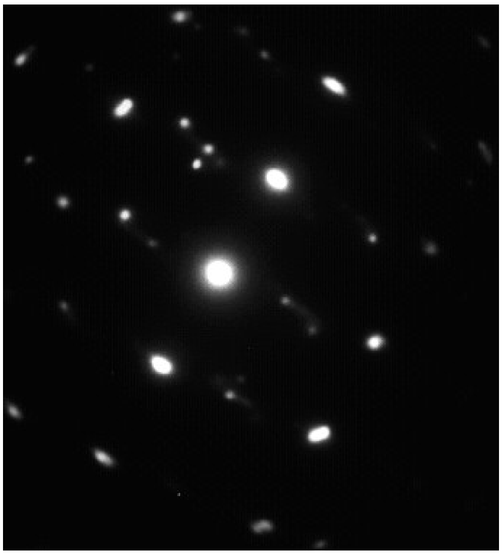

Figure 6.12(b)

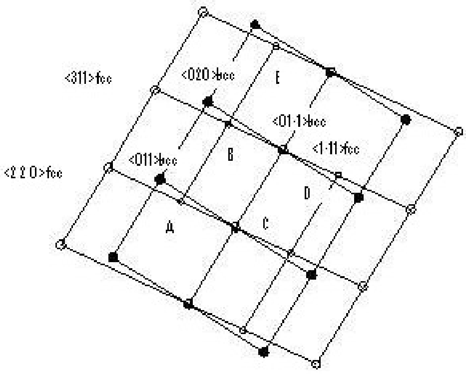

Figure 6.12(c)

The dark field images corresponding to the spots $\langle 0 \quad 2 \quad 0\rangle\alpha$ and $\langle 3 \quad 1 \quad 1\rangle\gamma$ are presented in Figure 6.12(d) and Figure 6.12(e).

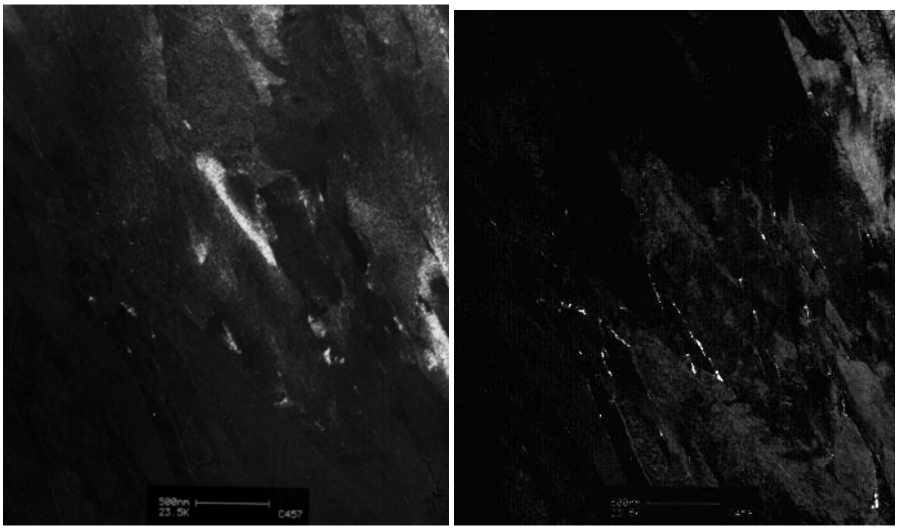

Figure 6.12(d) **Figure 6.12(e)**

Figure 6.12(d): Dark field image from the spot $\langle 0 \quad 2 \quad 0\rangle\alpha$ showing the martensite. **Figure 6.12(e)** from the spot $\langle 3 \quad 1 \quad 1\rangle\gamma$ showing the retained austenite

The N-W orientation relationship seems to prevail in these martensitic armour steels where the M_s temperature is lower than 200°C. The orientation relationship deviates from the N-W when the Ms temperature is higher. Spots suggesting autotempering appear in steels with M_s temperatures higher than 170°C.